Determination of the number of ψ(3686) events at BESIII*

Determination of the number of ψ(3686) events at BESIII*

M. Ablikim(麦迪娜)[1] M. N. Achasov[8,c] X. C. Ai(艾小聪)[1] D. J. Ambrose[41] A. Amoroso[45A,45C] F. F. An(安芬芬)[1] Q. An(安琪)[42] J. Z. Bai(白景芝)[1] R. Baldini Ferroli[19A] Y. Ban(班勇)[29] J. V. Bennett[18] M. Bertani[19A] J. M. Bian(边渐鸣)[40] E. Boger[21,a] O. Bondarenko[23] I. Boyko[21] R. A. Briere[4] H. Cai(蔡浩)[47] X. Cai(蔡啸)[1] O. Cakir[37A] A. Calcaterra[19A] G. F. Cao(曹国富)[1,38] S. A. Cetin[37B] J. F. Chang(常劲帆)[1] G. Chelkov[21,a,b] G. Chen(陈刚)[1] H. S. Chen(陈和生)[1,38] J. C. Chen(陈江川)[1] M. L. Chen(陈玛丽)[1] S. J. Chen(陈申见)[27] X. Chen(谌炫)[1] X. R. Chen(陈旭荣)[24] Y. B. Chen(陈元柏)[1] X. K. Chu(褚新坤)[29] Y. P. Chu(初元萍)[1] D. Cronin-Hennessy[40] H. L. Dai(代洪亮)[1] J. P. Dai(代建平)[1] D. Dedovich[21] Z. Y. Deng(邓子艳)[1] A. Denig[20] I. Denysenko[21] M. Destefanis[45A,45C] Y. Ding(丁勇)[25] C. Dong(董超)[28] J. Dong(董静)[1] L. Y. Dong(董燎原)[1,38] M. Y. Dong(董明义)[1] S. X. Du(杜书先)[49] J. Z. Fan(范荆州)[36] J. Fang(方建)[1] S. S. Fang(房双世)[1,38] Y. Fang(方易)[1] L. Fava[45B,45C] F. Feldbauer[20] C. Q. Feng(封常青)[42] C. D. Fu(傅成栋)[1] Q. Gao(高清)[1] Y. Gao(高原宁)[36] K. Goetzen[9] W. X. Gong(龚文煊)[1] W. Gradl[20] M. Greco[45A,45C] M. H. Gu(顾旻皓)[1] Y. T. Gu(顾运厅)[11] Y. H. Guan(管颖慧)[1] A. Q. Guo(郭爱强)[1] Y. P. Guo(郭玉萍)[20] Y. L. Han(韩艳良)[1] F. A. Harris[39] K. L. He(何康林)[1,38] M. He(何苗)[1] T. Held[3] Y. K. Heng(衡月昆)[1] Z. L. Hou(侯治龙)[1] H. M. Hu(胡海明)[1,38] T. Hu(胡涛)[1] G. S. Huang(黄光顺)[42] J. S. Huang(黄金书)[14] L. Huang(黄亮)[1] X. T. Huang(黄性涛)[31] T. Hussain[44] Q. Ji(纪全)[1] Q. P. Ji(姬清平)[28] X. B. Ji(季晓斌)[1,38] X. L. Ji(季筱璐)[1] L. L. Jiang(姜丽丽)[1] X. S. Jiang(江晓山)[1] J. B. Jiao(焦健斌)[31] Z. Jiao(焦铮)[16] D. P. Jin(金大鹏)[1] S. Jin(金山)[1,38] T. Johansson[46] N. Kalantar-Nayestanaki[23] X. L. Kang(康晓琳)[1] X. S. Kang(康晓珅)[28] M. Kavatsyuk[23] B. Kloss[20] B. Kopf[3] M. Kornicer[39] A. Kupsc[46] W. Kühn[22] W. Lai(赖蔚)[1] J. S. Lange[22] M. Lara[18] P. Larin[13] C. H. Li(李春花)[1] Cheng Li(李澄)[42] D. M. Li(李德民)[49] F. Li(李飞)[1] G. Li(李刚)[1] H. B. Li(李海波)[1,38] J. C. Li(李家才)[1] Kang Li(李康)[12] Ke Li(李科)[31] Lei Li(李蕾)[1] P. R. Li(李培荣)[6,38] Q. J. Li(李秋菊)[1] W. D. Li(李卫东)[1,38] W. G. Li(李卫国)[1] X. L. Li(李晓玲)[31] X. N. Li(李小男)[1] X. Q. Li(李学潜)[28] X. R. Li(李秀荣)[30] Z. B. Li(李志兵)[35] H. Liang(梁昊)[42] Y. F. Liang(梁勇飞)[33] Y. T. Liang(梁羽铁)[22] G. R. Liao(廖广睿)[10] D. X. Lin(林德旭)[13] B. J. Liu(刘北江)[1] C. X. Liu(刘春秀)[1] F. H. Liu(刘福虎)[32] Fang Liu(刘芳)[1] Feng Liu(刘峰)[5] H. B. Liu(刘宏邦)[11] H. M. Liu(刘怀民)[1,38] Huihui Liu(刘汇慧)[15] J. Liu(刘杰)[1] J. P. Liu(刘觉平)[47] K. Liu(刘凯)[36] K. Y. Liu(刘魁勇)[25] Q. Liu(刘倩)[38] S. B. Liu(刘树彬)[42] X. Liu(刘翔)[24] Y. B. Liu(刘玉斌)[28] Z. A. Liu(刘振安)[1] Zhiqiang Liu(刘志强)[1] Zhiqing Liu(刘智青)[20] H. Loehner[23] X. C. Lou(娄辛丑)[1] H. J. Lu(吕海江)[16] H. L. Lu(卢怀乐)[1] J. G. Lu(吕军光)[1] Y. Lu(卢宇)[1] Y. P. Lu(卢云鹏)[1] C. L. Luo(罗成林)[26] M. X. Luo(罗民兴)[48] T. Luo[39] X. L. Luo(罗小兰)[1] M. Lv(吕蒙)[1] X. R. Lyu(吕晓睿)[38] F. C. Ma(马凤才)[25] H. L. Ma(马海龙)[1] Q. M. Ma(马秋梅)[1] S. Ma(马斯)[1] T. Ma(马天)[1] X. Y. Ma(马骁妍)[1] F. E. Maas[13] M. Maggiora[45A,45C] Y. J. Mao(冒亚军)[29] Z. P. Mao(毛泽普)[1] J. G. Messchendorp[23] J. Min(闵建)[1] T. J. Min(闵天觉)[1] R. E. Mitchell[18] X. H. Mo(莫晓虎)[1] Y. J. Mo(莫玉俊)[5] C. Morales Morales[13] K. Moriya[18] N. Yu. Muchnoi[8,c] H. Muramatsu[40] Y. Nefedov[21] I. B. Nikolaev[8,c] Z. Ning(宁哲)[1] S. Nisar[7] S. L. Niu(牛顺利)[1] X. Y. Niu(牛讯伊)[1,38] S. L. Olsen(馬鵬)[30,g] Q. Ouyang(欧阳群)[1] S. Pacetti[19B] M. Pelizaeus[3] H. P. Peng(彭海平)[42] K. Peters[9,e] J. L. Ping(平加伦)[26] R. G. Ping(平荣刚)[1,38] R. Poling[40] M. Qi(祁鸣)[27] S. Qian(钱森)[1] C. F. Qiao(乔从丰)[38] X. S. Qin(秦小帅)[1] Z. H. Qin(秦中华)[1] J. F. Qiu(邱进发)[1] K. H. Rashid[44,f] C. F. Redmer[20] M. Ripka[20] G. Rong(荣刚)[1,38] A. Sarantsev[21,d] K. Schoenning[46] W. Shan(单葳)[29] M. Shao(邵明)[42] C. P. Shen(沈成平)[2] X. Y. Shen(沈肖雁)[1,38] H. Y. Sheng(盛华义)[1] M. R. Shepherd[18] W. M. Song(宋维民)[1] X. Y. Song(宋欣颖)[1] S. Sosio[45A,45C] S. Spataro[45A,45C] G. X. Sun(孙功星)[1] J. F. Sun(孙俊峰)[14] S. S. Sun(孙胜森)[1,38] Y. J. Sun(孙勇杰)[42] Y. Z. Sun(孙永昭)[1] Z. J. Sun(孙志嘉)[1] C. J. Tang(唐昌建)[33] X. Tang(唐晓)[1] I. Tapan[37C]

Received 13 September 2017, Revised 2 December 2017, Published online 5 January 2018

∗ Supported by the Ministry of Science and Technology of China (2009CB825200), National Natural Science Foundation of China (NSFC) (11235011, 11322544, 11335008, 11425524, 11475207), the Chinese Academy of Sciences (CAS) Large-Scale Scientific Facility Program, the Collaborative Innovation Center for Particles and Interactions (CICPI), Joint Large-Scale Scientific Facility Funds of the NSFC and CAS (11179014), Joint Large-Scale Scientific Facility Funds of the NSFC and CAS (11179007, U1232201, U1532257, U1532258), Joint Funds of the National Natural Science Foundation of China (11079008), CAS (KJCX2-YW-N29, KJCX2-YW-N45), 100 Talents Program of CAS, National 1000 Talents Program of China, German Research Foundation DFG (Collaborative Research Center CRC 1044), Istituto Nazionale di Fisica Nucleare, Italy, Koninklijke Nederlandse Akademie van Wetenschappen (KNAW) (530-4CDP03), Ministry of Development of Turkey (DPT2006K-120470), National Natural Science Foundation of China (11205082), The Swedish Research Council, U. S. Department of Energy (DE-FG02-05ER41374, DE-SC-0010118, DE-SC-0010504), U.S. National Science Foundation, University of Groningen (RuG) and the Helmholtzzentrum fuer Schwerionenforschung GmbH (GSI), Darmstadt, WCU Program of National Research Foundation of Korea (R32-2008-000-10155-0)

E. H. Thorndike[41] D. Toth[40] I. Uman[37D] G. S. Varner[39] B. Wang(王斌)[28] D. Wang(王东)[29] D. Y. Wang(王大勇)[29] K. Wang(王科)[1] L. L. Wang(王亮亮)[1] L. S. Wang(王灵淑)[1] M. Wang(王萌)[31] P. Wang(王平)[1] P. L. Wang(王佩良)[1] Q. J. Wang(王庆娟)[1] W. Wang(王炜)[1] X. F. Wang(王雄飞)[36] Y. D. Wang(Yadi)[19A] Y. F. Wang(王贻芳)[1] Y. Q. Wang(王亚乾)[20] Z. Wang(王铮)[1] Z. G. Wang(王志刚)[1] Z. Y. Wang(王至勇)[1] D. H. Wei(魏代会)[10] P. Weidenkaff[20] S. P. Wen(文硕频)[1] U. Wiedner[3] M. Wolke[46] L. H. Wu(伍灵慧)[1] Z. Wu(吴智)[1] L. G. Xia(夏力钢)[36] Y. Xia(夏宇)[17] D. Xiao(肖栋)[1] Z. J. Xiao(肖振军)[26] Y. G. Xie(谢宇广)[1] Q. L. Xiu(修青磊)[1] G. F. Xu(许国发)[1] L. Xu(徐雷)[1] Q. J. Xu(徐庆君)[12] Q. N. Xu(徐庆年)[38] X. P. Xu(徐新平)[34] W. B. Yan(鄢文标)[42] Y. H. Yan(颜永红)[17] H. X. Yang(杨洪勋)[1] Y. Yang(杨迎)[5] Y. X. Yang(杨永栩)[10] H. Ye(叶桦)[1] M. Ye(叶梅)[1] M. H. Ye(叶铭汉)[6] B. X. Yu(俞伯祥)[1] C. X. Yu(喻纯旭)[28] J. S. Yu(俞洁晟)[24] C. Z. Yuan(苑长征)[1,38] Y. Yuan(袁野)[1] A. A. Zafar[44] Y. Zeng(曾云)[17] B. X. Zhang(张丙新)[1] B. Y. Zhang(张炳云)[1] C. C. Zhang(张长春)[1] D. H. Zhang(张达华)[1] H. H. Zhang(张宏浩)[35] H. Y. Zhang(章红宇)[1] J. J. Zhang(张佳佳)[1] J. Q. Zhang(张敬庆)[1] J. W. Zhang(张家文)[1] J. Y. Zhang(张建勇)[1] J. Z. Zhang(张景芝)[1,38] L. Zhang(张磊)[1] R. Zhang(张瑞)[38] S. H. Zhang(张书华)[1] X. J. Zhang(张晓杰)[1] X. Y. Zhang(张学尧)[31] Y. H. Zhang(张银鸿)[1] Yao Zhang(张瑶)[1] Z. H. Zhang(张正好)[5] Z. P. Zhang(张子平)[42] Z. Y. Zhang(张振宇)[47] G. Zhao(赵光)[1] J. W. Zhao(赵京伟)[1] J. Z. Zhao(赵京周)[1] Lei Zhao(赵雷)[42] Ling Zhao(赵玲)[1] M. G. Zhao(赵明刚)[28] Q. Zhao(赵强)[1] Q. W. Zhao(赵庆旺)[1] S. J. Zhao(赵书俊)[49] T. C. Zhao(赵天池)[1] Y. B. Zhao(赵豫斌)[1] Z. G. Zhao(赵政国)[42] A. Zhemchugov[21,a] B. Zheng(郑波)[43] J. P. Zheng(郑建平)[1] Y. H. Zheng(郑阳恒)[38] B. Zhong(钟彬)[26] L. Zhou(周莉)[1] X. Zhou(周详)[47] X. K. Zhou(周晓康)[38] X. R. Zhou(周小蓉)[42] X. Y. Zhou(周兴玉)[1] K. Zhu(朱凯)[1] K. J. Zhu(朱科军)[1] X. L. Zhu(朱相雷)[36] Y. C. Zhu(朱莹春)[42] Y. S. Zhu(朱永生)[1,38] Z. A. Zhu(朱自安)[1,38] J. Zhuang(庄建)[1] B. S. Zou(邹冰松)[1] J. H. Zou(邹佳恒)[1]

(BESIII Collaboration)

[1] Institute of High Energy Physics, Beijing 100049, China
[2] Beihang University, Beijing 100191, China
[3] Beijing Institute of Petrochemical Technology, Beijing 102617, China
[4] Bochum Ruhr-University, D-44780 Bochum, Germany
[5] Carnegie Mellon University, Pittsburgh, Pennsylvania 15213, USA
[6] Central China Normal University, Wuhan 430079, China
[7] China Center of Advanced Science and Technology, Beijing 100190, China
[8] COMSATS Institute of Information Technology, Lahore, Defence Road, Off Raiwind Road, 54000 Lahore, Pakistan
[9] G.I. Budker Institute of Nuclear Physics SB RAS (BINP), Novosibirsk 630090, Russia
[10] GSI Helmholtzcentre for Heavy Ion Research GmbH, D-64291 Darmstadt, Germany
[11] Guangxi Normal University, Guilin 541004, China
[12] Guangxi University, Nanning 530004, China
[13] Hangzhou Normal University, Hangzhou 310036, China
[14] Helmholtz Institute Mainz, Johann-Joachim-Becher-Weg 45, D-55099 Mainz, Germany
[15] Henan Normal University, Xinxiang 453007, China
[16] Henan University of Science and Technology, Luoyang 471003, China
[17] Huangshan College, Huangshan 245000, China
[18] Hunan University, Changsha 410082, China
[19] Indiana University, Bloomington, Indiana 47405, USA
[20] (A)INFN Laboratori Nazionali di Frascati, I-00044, Frascati, Italy; (B)INFN and University of Perugia, I-06100, Perugia, Italy
[21] (A)INFN Sezione di Ferrara, I-44122, Ferrara, Italy; (B)University of Ferrara, I-44122, Ferrara, Italy
[22] Johannes Gutenberg University of Mainz, Johann-Joachim-Becher-Weg 45, D-55099 Mainz, Germany
[23] Joint Institute for Nuclear Research, 141980 Dubna, Moscow region, Russia
[24] Justus-Liebig-Universitaet Giessen, II. Physikalisches Institut, Heinrich-Buff-Ring 16, D-35392 Giessen, Germany
[25] KVI-CART, University of Groningen, NL-9747 AA Groningen, The Netherlands
[26] Lanzhou University, Lanzhou 730000, China
[27] Liaoning University, Shenyang 110036, China
[28] Nanjing Normal University, Nanjing 210023, China
[29] Nanjing University, Nanjing 210093, China
[30] Nankai University, Tianjin 300071, China
[31] Peking University, Beijing 100871, China
[32] Seoul National University, Seoul, 151-747 Korea
[33] Shandong University, Jinan 250100, China
[34] Shanghai Jiao Tong University, Shanghai 200240, China
[35] Shanxi University, Taiyuan 030006, China
[36] Sichuan University, Chengdu 610064, China
[37] Soochow University, Suzhou 215006, China
[38] Sun Yat-Sen University, Guangzhou 510275, China
[39] Tsinghua University, Beijing 100084, China
[40] (A)Ankara University, 06100 Tandogan, Ankara, Turkey; (B)Istanbul Bilgi University, 34060 Eyup, Istanbul, Turkey; (C)Uludag University, 16059 Bursa, Turkey; (D)Near East University, Nicosia, North Cyprus, Mersin 10, Turkey
[41] University of Chinese Academy of Sciences, Beijing 100049, China

[42] University of Hawaii, Honolulu, Hawaii 96822, USA
[43] University of Minnesota, Minneapolis, Minnesota 55455, USA
[44] University of Rochester, Rochester, New York 14627, USA
[45] University of Science and Technology Liaoning, Anshan 114051, China
[46] University of Science and Technology of China, Hefei 230026, China
[47] University of South China, Hengyang 421001, China
[48] University of the Punjab, Lahore-54590, Pakistan
[49] (A)University of Turin, I-10125, Turin, Italy; (B)University of Eastern Piedmont, I-15121, Alessandria, Italy; (C)INFN, I-10125, Turin, Italy
[50] Uppsala University, Box 516, SE-75120 Uppsala, Sweden
[51] Wuhan University, Wuhan 430072, China
[52] Zhejiang University, Hangzhou 310027, China
[53] Zhengzhou University, Zhengzhou 450001, China

[a] Also at State Key Laboratory of Particle Detection and Electronics, Beijing 100049, Hefei 230026, China
[b] Also at Bogazici University, 34342 Istanbul, Turkey
[c] Also at the Moscow Institute of Physics and Technology, Moscow 141700, Russia
[d] Also at the Functional Electronics Laboratory, Tomsk State University, Tomsk, 634050, Russia
[e] Also at the Novosibirsk State University, Novosibirsk, 630090, Russia
[f] Also at the NRC "Kurchatov Institute", PNPI, 188300, Gatchina, Russia
[g] Also at University of Texas at Dallas, Richardson, Texas 75083, USA
[h] Also at Istanbul Arel University, 34295 Istanbul, Turkey
[i] Also at Goethe University Frankfurt, 60323 Frankfurt am Main, Germany

Abstract: The numbers of ψ(3686) events accumulated by the BESIII detector for the data taken during 2009 and 2012 are determined to be $(107.0\pm0.8)\times10^6$ and $(341.1\pm2.1)\times10^6$, respectively, by counting inclusive hadronic events, where the uncertainties are systematic and the statistical uncertainties are negligible. The number of events for the sample taken in 2009 is consistent with that of the previous measurement. The total number of ψ(3686) events for the two data taking periods is $(448.1\pm2.9)\times10^6$.

Keywords: ψ(3686), inclusive process, hadronic events, Bhabha process

PACS: 13.25.Gv, 13.66.Bc, 13.20.Gd **DOI:** 10.1088/1674-1137/42/2/023001

1 Introduction

During two data taking periods, one in 2009 and one in 2012, the BESIII experiment accumulated the world's largest ψ(3686) data sample produced in electron-positron collisions, which provides an excellent resource to precisely study ψ(3686) transitions and decays and those of daughter charmonium states, *e.g.* χ_{cJ},h_c, and η_c, as well as to search for rare decays for physics beyond the standard model. The number of ψ(3686) events, $N_{\psi(3686)}$, is a crucial parameter, and its precision will directly affect the accuracy of these measurements.

In this paper, we present the determination of $N_{\psi(3686)}$ using inclusive ψ(3686) hadronic decays, whose branching fraction is known rather precisely, $(97.85\pm0.13)\%$ [1]. In the analysis, the QED background yield under the ψ(3686) peak is evaluated by analyzing the two sets of off-resonance data taken close in time with the peak samples, *i.e.* center-of-mass energy $\sqrt{s}=3.65$ GeV collected in 2009 and four energy points ranging from 3.542 to 3.600 GeV collected in 2012 for a τ-mass scan. The strategy for the background estimation was successfully used in our previous measurement of the number of ψ(3686) events collected in 2009 [2].

2 BESIII detector and Monte Carlo simulation

BEPCII is a double-ring e^+e^- collider that has reached a peak luminosity of 1×10^{33} cm^{-2}s^{-1} at $\sqrt{s}=$ 3.773 GeV. The cylindrical core of the BESIII detector consists of a helium-based main drift chamber (MDC), a plastic scintillator time-of-flight (TOF) system, and a CsI(Tl) electromagnetic calorimeter (EMC), which are all enclosed in a superconducting solenoid magnet with a field strength of 1.0 T (0.9 T in 2012). The solenoid is supported by an octagonal flux-return yoke with resistive plate counter modules interleaved with steel as a muon identifier. The acceptance for charged particles and photons is 93% over the 4π stereo angle. The charged-particle momentum resolution at 1 GeV/c is 0.5%, and the photon energy resolution at 1 GeV is 2.5% (5%) in the barrel (end-caps) of the EMC. More details about the apparatus can be found in Ref. [3]. The MDC encountered the Malter effect [4] due to cathode aging during ψ(3686) data taking in 2012. This effect was suppressed by mixing about 0.2% water vapor into the MDC operating gas [5] and can be well modeled by Monte Carlo (MC) simulation. The other sub-detectors worked well during 2009 and 2012.

The BESIII detector is modeled with a MC simulation based on GEANT4 [6]. The $\psi(3686)$ produced in the electron-positron collisions are simulated with the generator KKMC [7], which includes the beam energy spread according to the measurement of BEPCII and the effect of initial state radiation (ISR). The known decay modes of $\psi(3686)$ are generated with EVTGEN [8] according to the branching fractions in the Particle Data Group, PDG [1], while the remaining unknown decays are simulated using the LUNDCHARM model [9]. The MC events are generated with mixing of randomly triggered events (non-physical events from collision) in data taking to take into account the possible effects from beam-related backgrounds, cosmic rays, and electronic noise.

3 Event selection

The data collected at the $\psi(3686)$ peak includes several different processes, *i.e.*, $\psi(3686)$ decays to hadrons or lepton pairs (e^+e^-, $\mu^+\mu^-$, and $\tau^+\tau^-$), radiative return to the J/ψ, J/ψ decay due to the extended tail of the J/ψ line shape, and non-resonant (QED) processes, namely continuum background, including $e^+e^-\to\gamma^*\to$ hadrons, lepton pairs, and $e^+e^-\to e^+e^-+X$ (X=hadrons, lepton pairs). The data also contains non-collision events, *e.g.* cosmic rays, beam-associated backgrounds, and electronic noise. The process of interest in this analysis is $\psi(3686)$ decaying into hadrons.

Event selection includes track and photon level selection and event level selection. Charged tracks are required to be within 1 cm of the beam line in the plane perpendicular to the beam and within ±10 cm from the Interaction Point (IP) in the beam direction. Showers reconstructed in the EMC barrel region ($|\cos\theta|<0.80$) must have a minimum energy of 25 MeV, while those in the end-caps ($0.86<|\cos\theta|<0.92$) must have at least 50 MeV. The photons in the polar angle range between the barrel and end-caps are excluded due to the poor resolution. A requirement of the EMC cluster timing [0, 700] ns is applied to suppress electronic noise and energy deposits unrelated to the event.

At least one charged track is required for each candidate event. In the following, the selected events are classified into three categories according to the multiplicity of good charged tracks, *i.e.*, $N_{\rm good}=1$, $N_{\rm good}=2$, and $N_{\rm good}>2$, and named type-I, II, and III, respectively.

For type-III events, no further selection criteria are required. For type-II events, the momentum of each track is required to be less than 1.7 GeV/c and the opening angle (Δ_α) between the two charged tracks is required to be less than 176° to suppress Bhabha and dimuon backgrounds. Figures 1 and 2 show the scatter plots of the momentum of the first charged track versus that of the second charged track, and the distribution of the opening angle between the two charged tracks for the type-II candidates from simulated Bhabha (top) and inclusive $\psi(3686)$ (bottom) MC events, respectively. Further, an energy fraction requirement $E_{\rm visible}/E_{\rm cm}>0.4$ is applied to suppress the low energy background (LEB), comprised mostly of $e^+e^-\to e^+e^-+X$ and double ISR events ($e^+e^-\to\gamma_{\rm ISR}\gamma_{\rm ISR}X$). Here, $E_{\rm visible}$ is the visible energy which is defined as the total energy of all charged tracks (calculated with the track momentum assuming the tracks to be pions) and neutral showers, and $E_{\rm cm}$ is the center-of-mass energy. Figure 3 (top) shows the $E_{\rm visible}/E_{\rm cm}$ distributions of the type-II events for the $\psi(3686)$ data and inclusive MC sample. The visible excess in data at low energy is from the LEB events. Unless noted, in all plots, the points with error bars are the $\psi(3686)$ data collected in 2012, and the histogram is the corresponding MC simulation.

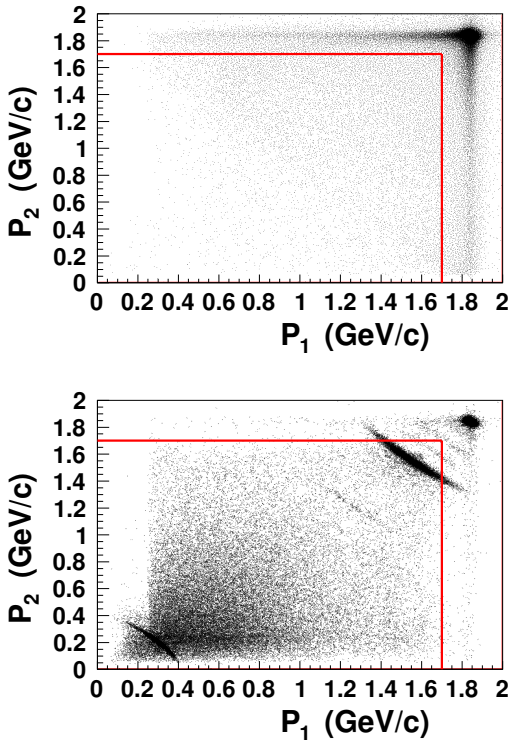

Fig. 1. (color online) Scatter plots of the momentum of the first charged track versus that of second charged track of type-II candidates for (top) Bhabha and (bottom) inclusive $\psi(3686)$ MC events. In the bottom plot, the event accumulation in the top-right corner comes from $\psi(3686)\to e^+e^-,\mu^+\mu^-$, while the different event bands nearby come from $\psi(3686)\to$neutral+J/ψ,$J/\psi\to e^+e^-,\mu^+\mu^-$ etc. The event band in the bottom-left comes from $\psi(3686)\to\pi^+\pi^-J/\psi$,$J/\psi\to e^+e^-,\mu^+\mu^-$ with lepton pairs missing. The horizontal and vertical lines show the selection requirements to suppress Bhabha and dimuon events.

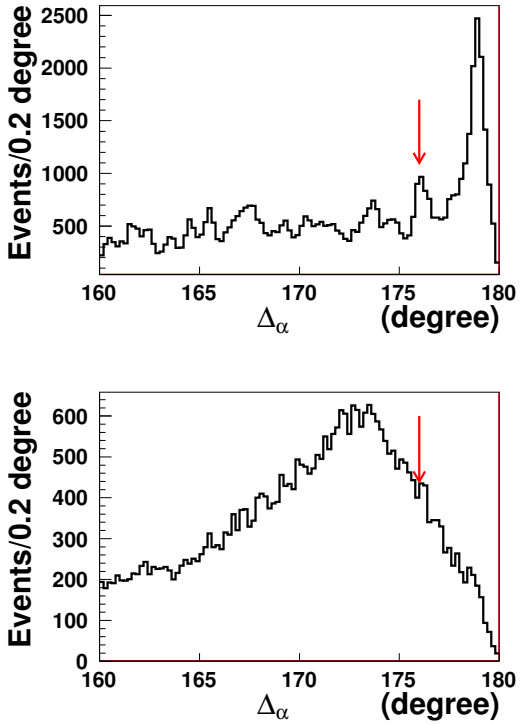

Fig. 2. (color online) Distributions of the opening angle between the two charged tracks for the type-II candidates from (top) Bhabha and (bottom) inclusive $\psi(3686)$ MC events after applying the momentum requirement for two tracks ($P<1.7$ GeV/c). The arrow shows the angle requirement used to suppress Bhabha and dimuon events.

For type-I events, at least two photons are required in an event. Compared to those events with high charged track multiplicity, the type-I sample has more background according to the vertex distribution of the charged tracks. Thus, a neutral hadron π^0 candidate is required to suppress the background events [10], where the π^0 candidate is reconstructed by any $\gamma\gamma$ combination. In an event, only the π^0 candidate with a mass closest to π^0 nominal value and satisfying $|M_{\gamma\gamma}-M_{\pi^0}|<0.015$ MeV/c^2 is kept for further analysis. Figure 4 shows the $M_{\gamma\gamma}$ distribution of selected π^0 candidates for type-I events. With the above selection criteria, the corresponding $E_{\rm visible}/E_{\rm cm}$ distributions of the candidate events for the $\psi(3686)$ data and inclusive MC sample are shown in Fig. 3 (bottom). An additional requirement $E_{\rm visible}/E_{\rm cm}>0.4$ is used to suppress the LEB events.

To discriminate the non-collision background from the collision events, the average vertex position in the Z direction is defined:

$$\bar{V}_Z=\frac{\sum_{i=1}^{N_{\rm good}} V_Z^i}{N_{\rm good}},$$

where V_Z^i is the (signed) distance along the beam direction between the point of closest approach of the i^{th} track and the IP. The $\bar{V}_Z$ distributions of the accepted hadronic events for the $\psi(3686)$ and off-resonance data are shown in the top and bottom plots of Fig. 5, respectively. The events satisfying $|\bar{V}_Z|<4$ cm are taken as signal, while the events in the sideband region $6<|\bar{V}_Z|<10$ cm are taken as non-collision background events. The number of the observed hadronic events ($N^{\rm obs}$) is obtained by counting the events in the signal region ($N_{\rm signal}$) and subtracting the non-collision background contribution estimated from the events in the sideband regions ($N_{\rm sideband}$) [11].

$$N^{\rm obs}=N_{\rm signal}-N_{\rm sideband}. \quad (1)$$

We also determine the number of hadronic events by fitting the $\bar{V}_Z$ distribution, where the signal event shape is described with a double Gaussian function, and the non-collision background is described with a second-order polynomial function. The resultant fit curves are shown in Fig. 5. This approach is used as a cross check and to estimate the corresponding systematic uncertainty.

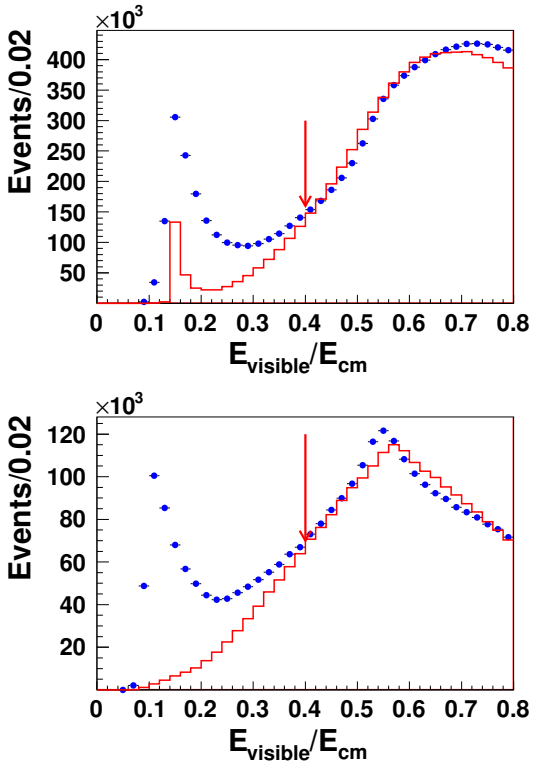

Fig. 3. (color online) Distribution of $E_{\rm visible}/E_{\rm cm}$ for the (top) type-II and (bottom) type-I events. The MC distributions are scaled to have the same number of entries as data for $E_{\rm visible}/E_{\rm cm}>0.4$.

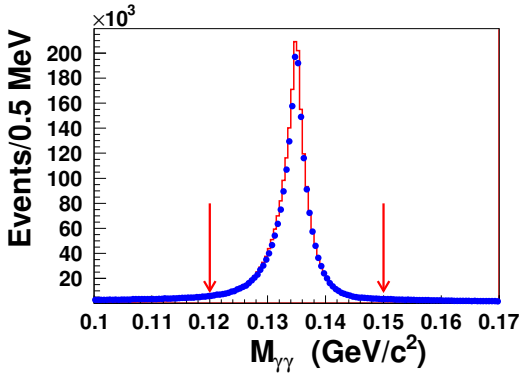

Fig. 4. (color online) Distribution of $M_{\gamma\gamma}$ in the π^0 mass region for the type-I events.

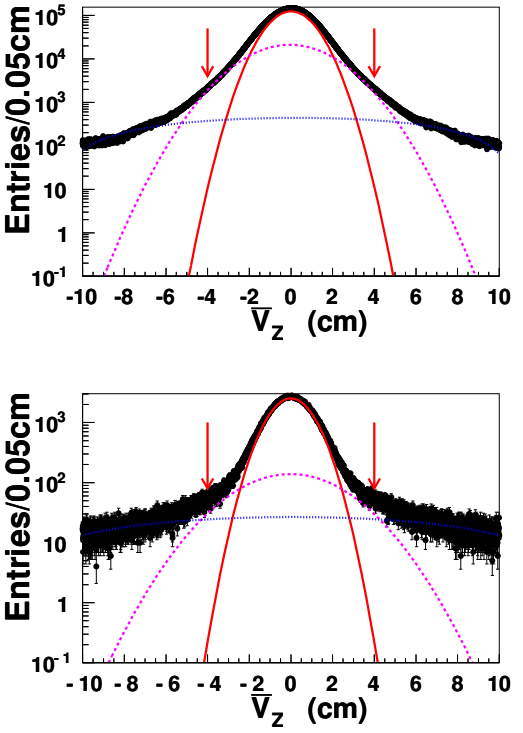

Fig. 5. (color online) Fits to the $\bar{V}_Z$ distributions of the accepted hadronic events in the (top) $\psi(3686)$ and (bottom) off-resonance data. The solid (red) and dashed (pink) curves show the double Gaussian line shapes for the signal and the dotted (blue) lines show the polynomial function for the non-collision events.

4 Background subtraction

In general, the observed number of QED events can be estimated by

$$N^{\rm QED}=\mathcal{L}\cdot\sigma\cdot\epsilon, \quad (2)$$

where $\mathcal{L}$ is the integrated luminosity, σ is the theoretical cross section for the QED processes, and ϵ is the efficiency determined from a MC simulation. Alternatively, as mentioned in Section 1, the off-resonance data samples can be used to estimate the continuum QED background yield. We apply the same approach to determine the yields of collision events and their uncertainties for the off-resonance data samples, which are dominated from the continuum QED processes. With the above method, the effect of QED background is independent of the MC simulation and the corresponding systematic bias is expected to be small.

For the $\psi(3686)$ and off-resonance data samples, the backgrounds from the radiative return to the J/ψ and J/ψ decay due to the extended tail are very similar due to the small difference in the center-of-mass energies. The total cross sections for these two processes are estimated to be 1.11 nb and 1.03 nb at the $\psi(3686)$ peak and the off-resonance energy point, respectively [12]. Detailed MC studies show that the efficiencies for the continuum processes are equal at these two energy points. Therefore, the off-resonance data can be employed to subtract both the continuum QED and J/ψ decay backgrounds using a scaling factor, f, determined from the integrated luminosity multiplied by a factor of $\frac{1}{s}$ to account for the energy dependence of the cross section,

$$f=\frac{\mathcal{L}_{\psi(3686)}}{\mathcal{L}_{\rm off-resonance}}\cdot\frac{s_{\rm off-resonance}}{s_{\psi(3686)}}, \quad (3)$$

where $\mathcal{L}_{\psi(3686)}$ and $\mathcal{L}_{\rm off-resonance}$ are the integrated luminosities for the $\psi(3686)$ and off-resonance data samples, respectively, and $s_{\psi(3686)}$ and $s_{\rm off-resonance}$ are the corresponding square of center-of-mass energies. For the τ-scan data, the average energy is determined to be $\sqrt{s}$ =3.572 GeV. The scaling factors f are determined to be 3.61 and 20.56 for the 2009 and 2012 data samples, respectively.

The integrated luminosities of the data samples taken at different energy points are determined from $e^+e^-\to\gamma\gamma$ events using the following selection criteria. Each event is required to have no good charged tracks and at least two showers. The energies for the two most energetic showers must be higher than 1.6 GeV, and the cosine of the polar angle of each electromagnetic shower must be within the region $|\cos\theta|<0.8$. The two most energetic showers in the $\psi(3686)$ rest frame must be back to back with azimuthal angles $||\phi_1-\phi_2|-180^\circ|<0.8^\circ$. The luminosities are $161.63\pm0.13\,{\rm pb}^{-1}$ and $506.92\pm0.23\,{\rm pb}^{-1}$ for $\psi(3686)$ data taken during 2009 and 2012, respectively, while $43.88\pm0.07\,{\rm pb}^{-1}$ and $23.14\pm0.05\,{\rm pb}^{-1}$ for off-resonance data taken at $\sqrt{s}$=3.65 GeV and for the τ-scan data set [13], respectively. Here, the errors are statistical only. The systematic uncertainties related to the luminosity almost cancel in calculating the scaling

factor due to the small difference between the energy points.

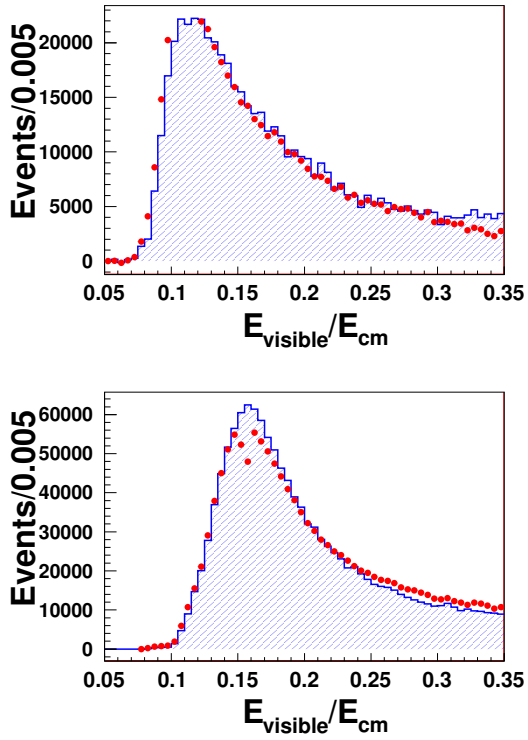

Fig. 6. (color online) Comparison of the $E_{\rm visible}/E_{\rm cm}$ distributions for the (top) type-I and (bottom) type-II LEB events between the $\psi(3686)$ and scaled off-resonance data. The dots with error bars are the former, and the shaded histogram is the latter.

In order to show that the shape of the LEB events in off-resonance data is consistent with that in the $\psi(3686)$ sample, and, therefore, scaled off-resonance data can be used to remove LEB background in the $\psi(3686)$ sample, we select an LEB sample by requiring $E_{\rm visible}/E_{\rm cm}<0.35$, where few QED events are expected. Figure 6 (top and bottom) shows the comparisons of the $E_{\rm visible}/E_{\rm cm}$ distributions for the type-I (top) and type-II (bottom) LEB events between the $\psi(3686)$ and the scaled off-resonance data samples taken in 2012. The ratios of the number of events between the $\psi(3686)$ peak and the off-resonance energy are 22.78 and 22.57 for the type I and type II events, respectively. Compared with the scaling factor obtained from the integrated luminosity normalization in Eq. (3), a difference of 10% is found for the type-I and type-II events. Similar differences are found for the 2009 data sample [2]. Since the fraction of LEB events in the selected sample is very small, the effect of this difference for the background estimation is negligible.

The cross sections for $e^+e^-\to\tau^+\tau^-$ are 0.67, 1.84, and 2.14 nb at the τ-scan energy ($\sqrt{s}$=3.572 GeV according to luminosity weighted average), $\sqrt{s}$=3.65 GeV and the $\psi(3686)$ peak, respectively. Since the above energy points are close to $\tau^+\tau^-$ mass threshold, the production cross section does not follow a $1/s$ distribution. Thus, only a part of the $e^+e^-\to\tau^+\tau^-$ background events is included in the off-resonance data samples. To correct for the full background from $e^+e^-\to\tau^+\tau^-$, we estimate the remaining contribution, $N^{\rm uncanceled}_{\tau^+\tau^-}$, using the detection efficiency from MC simulation and the cross section difference at off-resonance energy points and the $\psi(3686)$ peak, as well as the luminosity at the $\psi(3686)$ peak. The estimated values are shown in Table 1.

The small numbers of surviving events from $\psi(3686)\to e^+e^-$, $\mu^+\mu^-$, and $\tau^+\tau^-$ in data do not need to be explicitly subtracted since these leptonic $\psi(3686)$ decays have been included in the inclusive MC samples, and their effects are considered in the detection efficiency.

Table 1. Numbers of the observed hadronic events, $N^{\rm obs}_{\psi(3686)}(\times10^6)$, numbers of the observed hadronic events in off-resonance data, $N^{\rm obs}_{\rm off-resonance}(\times10^6)$, corresponding to the bottom plot in Fig. 5, numbers of the remaining $e^+e^-\to\tau^+\tau^-$ events after subtracting the normalized off-resonance data, $N^{\rm uncanceled}_{\tau^+\tau^-}(\times10^6)$, the detection efficiencies, ϵ, of $\psi(3686)\to$hadrons for different charged-track multiplicity requirements, and numbers of $\psi(3686)$ events, $N_{\psi(3686)}$ $(\times10^6)$.

multiplicity	$N_{\rm good}\geqslant1$		$N_{\rm good}\geqslant2$		$N_{\rm good}\geqslant3$	
year	2009	2012	2009	2012	2009	2012
$N^{\rm obs}_{\psi(3686)}$	107.72	343.51	103.72	329.04	82.28	259.98
$N^{\rm obs}_{\rm off-resonance}$	2.23	1.325	2.01	1.245	0.74	0.400
$N^{\rm uncanceled}_{\tau^+\tau^-}$	0.036	0.57	0.034	0.54	0.013	0.21
ϵ (%)	92.92	92.39	89.96	88.96	74.73	73.20
$N_{\psi(3686)}$	107.2	341.7	107.2	340.5	106.6	343.6

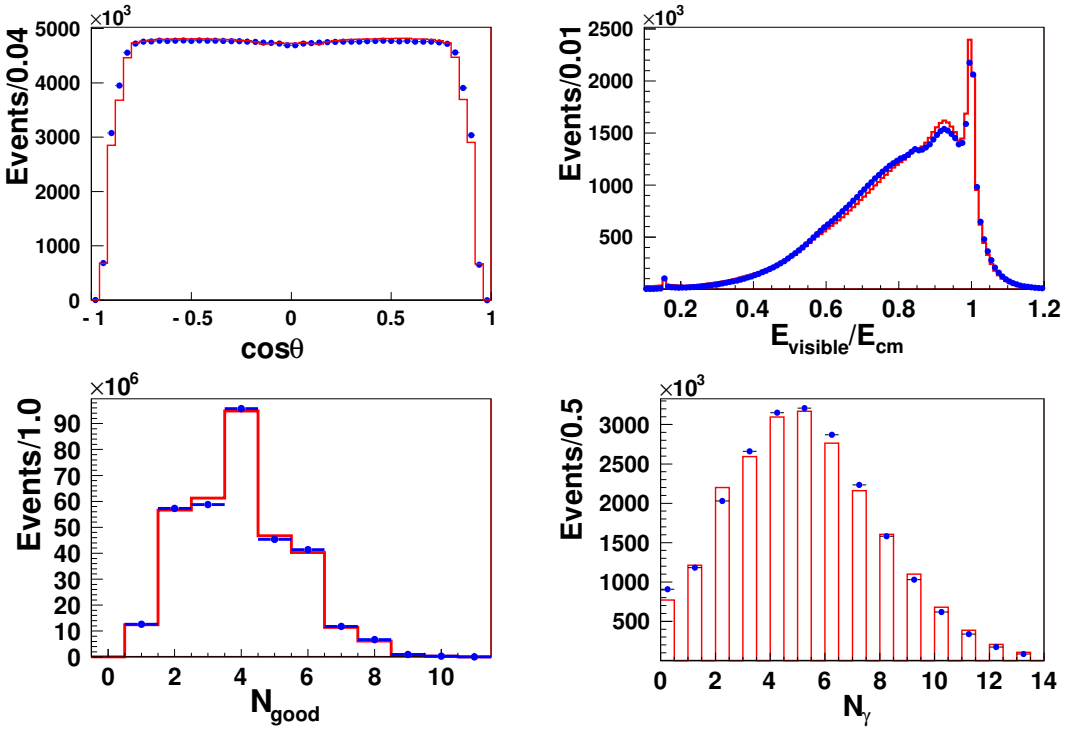

Fig. 7. (color online) Comparisons of data and MC simulation: (top-left) The cosθ distribution, (top-right) $E_{\rm visible}/E_{\rm cm}$ distribution, (bottom-left) charged-track multiplicity distribution, and (bottom-right) photon multiplicity distribution.

Table 1 also shows the numbers of the observed hadronic events for different charged-track multiplicity requirements of the $\psi(3686)$ ($N^{\rm obs}_{\psi(3686)}$) and off-resonance data ($N^{\rm obs}_{\rm off-resonance}$). The corresponding detection efficiencies of $\psi(3686)\to$ hadrons are determined with 363.7×10^6 $\psi(3686)$ inclusive MC events, and are also listed in this table. The branching fraction of $\psi(3686)\to$ hadrons is included in the efficiency. Figure 7 shows the comparisons for cosθ, $E_{\rm visible}/E_{\rm cm}$, charged-track multiplicity, and photon multiplicity distributions after background subtraction between data and MC simulation, and reasonable agreement between data and MC simulation is observed.

5 Numerical results

The number of $\psi(3686)$ events, $N_{\psi(3686)}$, can be calculated from

$$N_{\psi(3686)}=\frac{N^{\rm obs}_{\rm peak}-f\cdot N^{\rm obs}_{\rm off-resonance}-N^{\rm uncanceled}_{\tau^+\tau^-}}{\epsilon}. \quad (4)$$

With the numbers listed in Table 1, the numerical results for $N_{\psi(3686)}$ with different charged-track multiplicity requirements are calculated and listed in Table 1. There are slight differences between different multiplicity requirements due to the imperfect MC simulation of the charged track multiplicity. To obtain a more exact numerical result for $N_{\psi(3686)}$, an unfolding method is employed based on an efficiency matrix, whose matrix elements, ϵ_{ij}, represent the probability to observe i charged tracks for an event with j actual charged tracks. The efficiency matrix is determined from the inclusive MC samples. In practice, there are even numbers of charged tracks generated in an event due to charge conservation, while any number of charged tracks can be observed due to the reconstruction efficiency and backgrounds. Therefore, the true charged track multiplicity of the data sample is estimated from the observed multiplicity and the efficiency matrix by minimizing a χ^2 value, defined as

$$\chi^2=\sum_{i=1}^{10}\frac{\left(N_i^{\rm obs}-\sum\limits_{j=0}^{10}\epsilon_{ij}\cdot N_j\right)^2}{N_i^{\rm obs}}, \quad (5)$$

where the values $N^i_{\rm obs}(i=0,\ 1,\ 2,\cdots)$ are the observed multiplicities of charged tracks in data sample which correspond to the distribution in Fig. 7 (bottom-left, the points with error bars), while the values N_j ($j=$ 0, 2, 4,$\cdots$) are the true multiplicities of charged tracks in the data sample. They are the free parameters in the fit. For simplicity, the events with ten or more tracks are combined in a single value, N_{10}. The value of $N_{\psi(3686)}$ can be calculated by summing over all the obtained N_j. The results are 107.0×10^6 and 341.1×10^6 for the 2009

and 2012 data samples, respectively.

6 Systematic uncertainties

The systematic uncertainties in the $N_{\psi(3686)}$ measurement from different sources are described below and listed in Table 2. The total systematic uncertainty is determined by the quadratic sum of all individual values.

6.1 Polar angle

The polar angle acceptance for the charged tracks in the MDC is $|\cos\theta|<0.93$. From Fig. 7 (top-left), there is a slight difference between data and MC simulation at large polar angles. As a check, the requirement on the polar angle is changed to be $|\cos\theta|<0.8$. The difference in $N_{\psi(3686)}$ is taken as the uncertainty due to the requirement on the polar angle.

6.2 Tracking

A small difference (less than 1%) on the tracking efficiency between data and MC simulation is observed by various studies [14]. Assuming the average efficiency difference between data and MC simulation is 1% per track, the effect can be determined by randomly removing MC simulated tracks with a 1% probability. This results in a negligible difference in $N_{\psi(3686)}$, implying that $N_{\psi(3686)}$ is not sensitive to the tracking efficiency.

6.3 Charged-track multiplicity

The effect due to the simulation of the charged-track multiplicity has been taken into account by the unfolding method described above. By comparing the results between the direct calculation in Table 1 and the unfolding method including the $N_{\rm good}\leqslant 1$ events, there is a difference of 0.2% on $N_{\psi(3686)}$ for both the 2009 and 2012 data, which is taken as the uncertainty associated with the charged-track multiplicity.

6.4 Momentum and opening angle

For the type-II events, the requirements on the momentum of charged tracks and the opening angle between two charged tracks are applied to reject the sizable background from Bhabha and dimuon events. When the requirement of charged track momentum is changed from $P<1.7$ GeV/c to $P<1.55$ GeV/c, the resultant change in $N_{\psi(3686)}$ is negligible. When the requirement on opening angle between two charged tracks is changed from $\theta<176^\circ$ to $\theta<160^\circ$, the change in $N_{\psi(3686)}$ is negligibly small for the 2009 data and is 0.04% for the 2012 data. Figure 8 shows comparisons of the distributions of the momentum and the opening angle of the two charged tracks after background subtraction in the type-II events between the data and inclusive MC simulation.

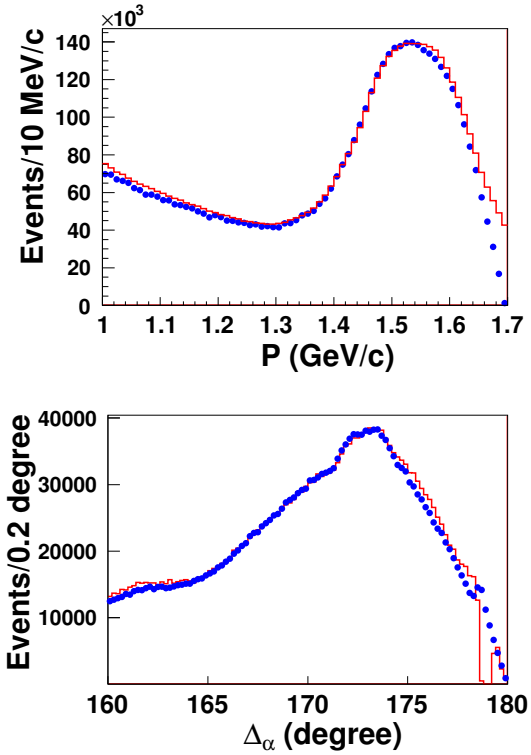

Fig. 8. (color online) Distributions of (top) charged track momentum and (bottom) opening angle between the two charged tracks for type-II events.

6.5 LEB contamination

$N_{\psi(3686)}$ is insensitive to the visible energy requirement. The uncertainty associated with the requirement $E_{\rm visble}/E_{\rm cm}>0.4$ is estimated by comparing the results with or without this requirement, and the difference on $N_{\psi(3686)}$ is assigned to be the corresponding uncertainty.

6.6 Determination of $N^{\rm obs}$

As mentioned as in Sec. 3, two methods are used to obtain $N^{\rm obs}$. The nominal method counts the numbers of events in the signal region and subtracts the number of background estimated in the sideband regions. The alternative method is performed by fitting the $\bar{V}_Z$ distribution. The resultant difference on $N^{\rm obs}$ between these two methods is taken as the uncertainty in the determination of $N^{\rm obs}$.

6.7 Vertex requirement

We repeat the analysis by changing the requirement $V_r<1$ cm to $V_r<2$ cm, and the change in $N_{\psi(3686)}$ is small and is taken as the systematic uncertainty. Similarly, we repeat the analysis by changing the requirement $|\bar{V}_Z|<10$cm to $|\bar{V}_Z|<20$cm, and find a negligible change in $N_{\psi(3686)}$.

6.8 Scaling factor

The scaling factor (f) for the background subtraction depends on the luminosity of the data samples. In the nominal analysis, the luminosity is estimated with $e^+e^- \to \gamma\gamma$ events. An alternative measurement of the luminosity is performed with large angle Bhabha events, and the scaling factor as well as $N_{\psi(3686)}$ are recalculated. The resultant difference in $N_{\psi(3686)}$ is found to be negligible, and the corresponding uncertainty is negligible.

6.9 Choice of sideband region

In the nominal analysis, we take $|\bar{V}_Z|<4$cm as the signal region and $6<|\bar{V}_Z|<10$cm as the sideband region. An alternative analysis is done shifting the sideband region outward by 1 cm, which is about 1σ of the $\bar{V}_Z$ resolution. The resulting difference in $N_{\psi(3686)}$ is taken as the systematic uncertainty.

6.10 π^0 mass requirement

The π^0 mass requirement is only applied for the type-I events. There is a slight change in $N_{\psi(3686)}$ when the mass window requirement is changed from $|M_{\gamma\gamma}-M_{\pi^0}|<0.015\,\mathrm{GeV}/c^2$ to $|M_{\gamma\gamma}-M_{\pi^0}|<0.025\,\mathrm{GeV}/c^2$. This difference is taken as the uncertainty due to the π^0 mass requirement.

6.11 Missing $N_{\rm good}=0$ hadronic events

A detailed topological analysis is performed for the events with $N_{\rm good}=0$ in the inclusive MC sample. Most of these events come from the well-known decay channels, such as $\psi(3686) \to X + J/\psi$ (where X denotes η,π^0,$\pi^0\pi^0$,$\gamma\gamma$ *etc.*) and $\psi(3686) \to e^+e^-$, $\mu^+\mu^-$. The fraction of these $N_{good}=0$ events in the inclusive MC sample is $\sim$2.0%, of which the pure neutral channels contribute about 1.0%. As shown in Fig. 7, the MC simulation models data well. Therefore, we investigate the pure neutral hadronic events, which are selected according to the following scheme. With the same charged track and shower selection criteria as above, we require $N_{\rm good}=0$ and $N_\gamma>3$. The latter requirement is used to suppress $e^+e^-\to\gamma\gamma$ and beam-associated background events. The same selection criteria are imposed on the off-resonance data and inclusive MC events. Figure 9 shows the distributions of the total energies in the EMC, $E_{\rm EMC}$, for the different data sets and inclusive MC sample. The peaking events around the center-of-mass energy are taken as the pure neutral hadronic candidates. As shown in Fig. 9, the number of signal events is determined by a fit of the $E_{\rm EMC}$ distribution. In this fit, the signal is described by a Crystal Ball function, the QED background in $\psi(3686)$ data is described by the shape of off-resonance data (off-resonance data at $\sqrt{s}=3.65\,\mathrm{GeV}$ or τ-scan data) after scaling for luminosity, and the other backgrounds are described by a polynomial function. For the 2012 data, the difference in the number of pure neutral hadronic events between the data and the inclusive MC simulation sample is 11% if the τ-scan data sample is taken as the off-resonance data to estimate the background function, as shown in Fig. 9 (top). However, this difference changes to 18% if we use the off-resonance data at $\sqrt{s}=3.65\,\mathrm{GeV}$ for the background function, as shown in Fig. 9 (middle). The larger difference is used to estimate the uncertainty conservatively. Since the fraction

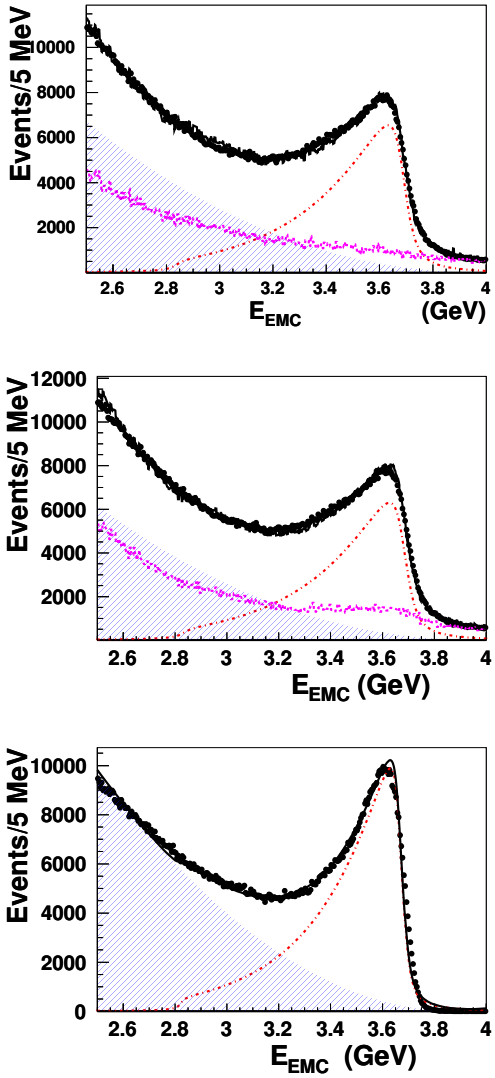

Fig. 9. (color online) Distributions of the total energies in the EMC for the $N_{\rm good}=0$ events for (top) the $\psi(3686)$ data with QED background approximated by the τ-scan data, (middle) the data taken at $\sqrt{s}$=3.65 GeV, and (bottom) the inclusive $\psi(3686)$ MC sample. The dot-dashed lines are the signal shapes of neutral $\psi(3686)$ decays and the shaded regions are the background shapes from $\psi(3686)$ decays. The dashed lines are the background shapes from QED processes.

Table 2. Systematic uncertainties (%).

source	2009	2012
polar angle	0.27	0.31
tracking	negligible	negligible
charged track multiplicity	0.20	0.19
momentum and opening angle	negligible	0.04
LEB contamination	negligible	0.09
$N^{\rm obs}$ determination	0.27	0.30
vertex requirement	0.32	0.21
scaling factor (f)	negligible	negligible
choice of sideband region	0.32	0.26
π^0 mass requirement	0.09	0.05
$N_{\rm good}=0$ events	0.25	0.18
MC modeling	negligible	negligible
trigger	negligible	negligible
$B(\psi(3686)\to$hadrons)	0.13	0.13
total	0.70	0.63

of the pure neutral hadronic events is about 1.0% of the total selected candidates, the uncertainty due to the missing $N_{\rm good}=0$ events should be less than $18\%\times1\%=0.18\%$ for the 2012 data. The same method is applied to the 2009 data samples, and the uncertainty is 0.25%, which is somewhat larger than the previous analysis [2].

6.12 MC modeling

The uncertainty due to the MC simulation of inclusive $\psi(3686)$ decays arises from sources such as the input of branching fractions, the angular distributions of the known and unknown decay modes, *etc.* These uncertainties have been covered by those from the charged-track multiplicity, missing of $N_{\rm good}=0$ events *etc.* Thus, no further uncertainty is assigned for the MC modeling.

6.13 Trigger

Based on the 2009 data, the trigger efficiency for the $N_{\rm good}\geqslant2$ (type-II and type-III) events is close to 100.0%, while it is 98.7% for the type-I events [15]. Since the fraction of type-I events is only about 3% of the total selected events, the uncertainty caused by the trigger is negligible for the 2009 data. As shown in Table 1, the fraction of type-I events in the 2012 data is the same as that in the 2009 data. Furthermore, an additional neutral trigger channel was added during 2012 data taking. Therefore, the trigger efficiency for the 2012 data is expected to be higher for type-I events than that for the 2009 data, and the uncertainty associated with the trigger is negligible.

6.14 $B(\psi(3686)\to$hadrons)

The uncertainty of the branching fraction for $\psi(3686)\to$hadrons is small, 0.13% [1] and taken as the uncertainty.

7 Summary

The number of $\psi(3686)$ events taken by BESIII in 2012 is measured to be $(341.1\pm2.1)\times10^6$ with the inclusive hadronic events, where the uncertainty is systematic and the statistical uncertainty is negligible. The number of $\psi(3686)$ events taken in 2009 is also updated to be $(107.0\pm0.8)\times10^6$, which is consistent within the uncertainty with respect to the previous measurement, and the improved precision is due to the refined offline software, MC tuning, and the improved method to determine $N_{\psi(3686)}$. Adding the results linearly yields the total number of $\psi(3686)$ events for the two runs to be $(448.1\pm2.9)\times10^6$. This work provides an important parameter for the studies of the decays of the $\psi(3686)$ and its daughters.

The BESIII collaboration thanks the staff of BEPCII and the computing center for their hard efforts.

References

1 C. Patrignani et al (Particle Data Group), Chin. Phy. C, 2016, **40**: 100001
2 M. Ablikim et al (BESIII Collaboration), Chin. Phys. C, 2013, **37**: 063001
3 M. Ablikim et al (BESIII Collaboration), Nucl. Instrum. Meth. A, 2010, **614**: 345
4 L. Malter, Phys. Rev., **50**(1): 48 (1936)
5 M. Y. Dong, et al Chin. Phys. C, 2016, **40**: 016001
6 S. Agostinelli et al (GEANT4 Collaboration), Nucl. Instrum. Meth. A, 2003, **506**: 250; J. Allison et al, IEEE Trans. Nucl. Sci., **53**: 270 (2006)
7 S. Jadach, B. F. L. Ward, and Z. Was, Comput. Phys. Commun., **130**: 260 (2000); S. Jadach, B. F. L. Ward, and Z. Was, Phys. Rev. D, **63**: 113009 (2001)
8 D. J. Lange et al, Nucl. Instrum. Meth. A, **462**: 152 (2001); R. G. Ping et al, Chin. Phys. C, **32**: 599 (2008)
9 J. C. Chen et al, Phys. Rev. D, **70**: 011102(R) (2005)
10 M. Ablikim et al (BES Collaboration), Phys. Lett. B, **677**: 239 (2009)
11 Y. Weng, et al Chin. Phys. C, **31**: 703 (2007)
12 M. Ablikim et al (BES Collaboration), Phys. Rev. Lett., **97**: 121801 (2006)
13 M. Ablikim et al (BESIII Collaboration), Phys. Rev. D, **90**: 012001 (2014)
14 M. Ablikim et al (BESIII Collaboration), Phys. Lett. B, **710**: 594 (2012)
15 N. Berger et al, Chin. Phys. C, **34**: 1779 (2010)